Room Temperature Lasing in Micro-Rings of Blended Core/Shell Quantum Dots

Zehua Ren（任则华）[1,#], Xiaoyu Wang（王小宇）[1,#], Zelei Chen（陈泽磊）[1], Dachuan Li（李大川）[1], Zhongmin Huang（黄钟民）[1], Gang Ni（倪刚）[1], Chuanxiang Sheng（盛传祥）[1,2], Jun Wang（王俊）[1,2,*]

[1] Key Laboratory of Micro & Nano Photonic Structures, Department of Optical Science and Engineering, College of Future Information Technology, Fudan University, Shanghai, 200433, China

[2] State Key Laboratory of Photovoltaic Science and Technology, Shanghai Key Laboratory of Metasurfaces for Light Manipulation, Fudan University, Shanghai, 200433, China

[#] *These authors contributed equally to this work.*

[*] Corresponding to: wangjunfd@fudan.edu.cn; wuyuchen@iccas.ac.cn

Abstract

Colloidal quantum dots (QDs) are nanoscale semiconductor particles with unique optical and electronic properties, widely used in optoelectronic fields as gain materials. Particularly in micro-lasers, the lasing investigation of blended core/shell QDs plays an important role in improving lasing performance and exciton dynamics. Here, we demonstrate room-temperature photonic lasing in blended QD micro-rings and reveal the mechanism of population inversion. High-quality micro-rings of red and green colloidal core/shell QDs and their blend are fabricated by utilizing the solution self-assembled patterning method. Steady-state and time-resolved spectral characterization illustrate the lasing of blended QD rings arising from the exciton transition of the 2S state, while the lasing of pure red and green QD rings with the 1S exciton transition. In blended QD rings, Förster resonance energy transfer (FRET) from green QDs to red QDs induces exciton redistribution and promotes exciton accumulation in the 2S state of red QDs rather than the 1S state, leading to population inversion and lasing emission. Our study of lasing behaviors and mechanisms for blended colloidal QD micro-rings paves a promising avenue toward further developing on-chip integrated QD lasing sources and optoelectronic devices.

Keywords: photonic lasing, microcavity, colloidal quantum dots, FRET

PACS: 42.55.Sa, 78.67.Hc, 42.60.Da

Introduction

Large-scale integration of high-performance optoelectronic devices has become increasingly important in recent years. Due to the unique electronic structures and optical properties, semiconductor nanomaterials with quantum confinement effects have attracted extensive attention[1,2]. Among them, quantum dots (QDs), as typical zero-dimensional semiconductor nanostructures, exhibit discrete energy levels and size-dependent optical properties, enabling tunable emission wavelengths and excellent photophysical performance[3-7]. Owing to their high photoluminescence quantum yield, low optical gain threshold, and narrow emission linewidth, QDs have emerged as promising gain media for nanoscale lasing devices[1,8-10]. Previous studies on colloidal QD lasers have mainly focused on stimulated emission from the lowest-energy 1S exciton transition, benefiting from its strong oscillator strength and favorable optical gain characteristics[11-13]. Various QD-based microcavities have demonstrated low-threshold lasing based on 1S exciton states, such as wire, disk, and ring resonators[14-16]. Under sufficiently high excitation densities, state filling of the lower-energy exciton states can further populate higher-energy states, giving rise to excited-state emission, stimulated emission, or optical gain[12,17,18]. These studies demonstrate the accessibility of higher-energy excitonic states under strong excitation. However, the selective regulation of the excitonic state that dominates the lasing process remains challenging.

Particularly, core/shell cadmium selenide/zinc sulfide (CdSe/ZnS) QDs have attracted extensive attention owing to their high PL quantum yield, excellent stability, and strong optical gain capability[19-22]. The ZnS shell effectively passivates surface defects and suppresses nonradiative recombination[23], making CdSe/ZnS QDs promising candidates for investigating exciton dynamics and lasing phenomena. Owing to quantum confinement, CdSe QDs possess discrete excitonic states, including the lowest-energy 1S state and higher-energy excited states[18,24-26]. Although higher-energy states can be populated through state filling under strong excitation, their rapid relaxation and the competition among population, optical gain, and loss make it difficult for a higher-energy transition to preferentially reach the lasing condition[27]. One

possible approach to regulating the exciton population is to construct QD heterostructures, in which interparticle energy transfer provides additional pathways for exciton redistribution[28-30]. In donor-acceptor QD systems, FRET enables nanoscale exciton transfer and can modify exciton relaxation pathways and population distributions[31,32]. Recent studies have further employed FRET to enhance optical gain and lasing performance in donor-acceptor QD systems[33,34]. These studies mainly focused on gain enhancement and lasing-performance improvement, whereas the use of FRET-mediated exciton redistribution to regulate which excitonic transition preferentially reaches the lasing condition remains insufficiently explored. Therefore, the use of FRET-mediated exciton redistribution to regulate the preferential lasing exciton state, particularly to enable higher-energy lasing, remains insufficiently explored. In addition to exciton-population regulation, integrating QDs with microcavities provide strong optical confinement and feedback, which further affects the gain-loss competition among different excitonic transitions[35]. In ring resonator systems, whispering gallery modes (WGMs) offer enhanced optical confinement and resonant optical feedback, which not only improve photon extraction efficiency but also enable precise control over the emitted optical mode[14,15,36,37]. However, how to synergistically manipulate exciton population redistribution, state filling effects, and cavity-enhanced optical feedback to achieve selective lasing from higher-energy excitonic states remains an open question.

In this study, we have fabricated uniform-size and high-quality micro-ring arrays with colloidal CdSe/ZnS QDs and their blend and realized lasing emission in different-size ring resonators. By the steady-state PL spectral characterizations, we observed the emergence of a higher-energy 2S-state exciton transition in pure red QDs with the carrier density increasing, due to the filling effect of quantum-confined discrete energy levels. Based on this phenomenon and the heterojunction band structure formed in the blend of green (donor) and red (acceptor) QDs, we realize lasing emission at the 2S state of acceptors in blend micro-rings. Furthermore, time-resolved PL measurements reveal that resonance energy transfer results in a rapid exciton accumulation on the 2S

state of acceptors in blend QDs, which adjusts lasing population inversion and differs from the 1S-state lasing of pure red and green QDs. Our findings provide a feasible approach to modulating the lasing population in self-assembled blended QD optical resonators and contribute to the applications of high-performance optoelectronic lasers and display devices.

Results and discussion

Optical characterizations and the fabrication of CdSe/ZnS QD micro-rings

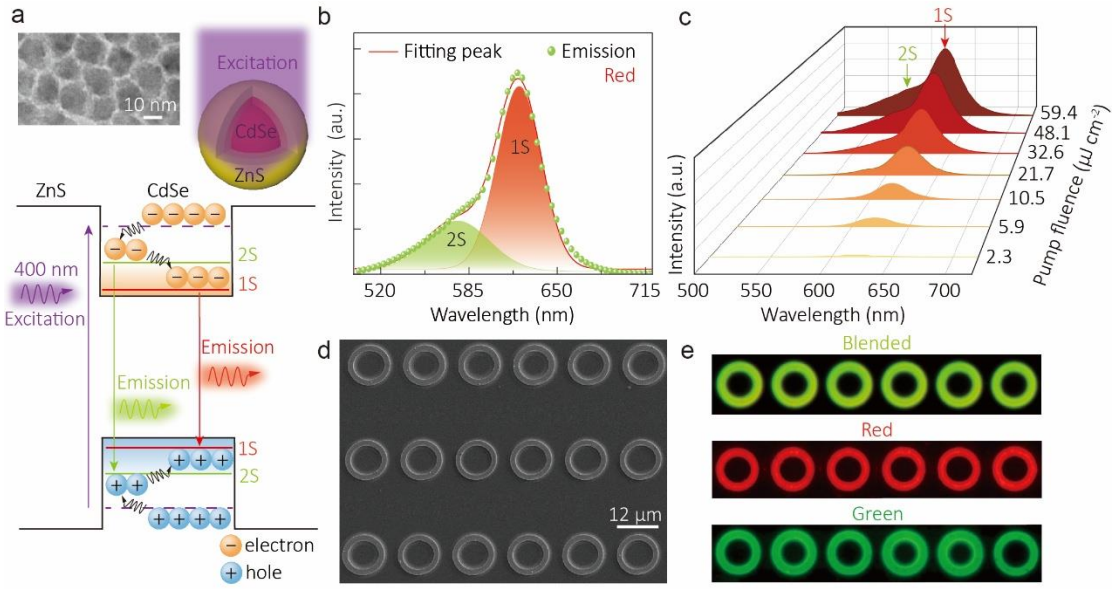


Fig. 1. Optical characterizations and fabrications of CdSe/ZnS core/shell QDs. (a) Schematic of photoluminescence of red QDs. The inset is a transmission electron microscope. **(b)** PL spectra of red QDs at RT, showing two peaks. The red and green fitted peaks are from the 1S and 2S transition, respectively. **(c)** The power-dependent PL spectra of red QDs at RT. **(d)** Scanning electron microscope of an array of QD micro-ring resonators. The ring diameter and width are 12 μm and 1.5 μm. Scale bar: 12 μm. **(e)** Fluorescence microscope images of red and green and blended QD micro-ring resonators.

The simple solution patterning method, which allows the manufacture of finely structured surfaces, can be used to fabricate large-area micro-scale resonant cavities[38]. The detailed methodological procedures are presented in the supplementary information (SI). We apply this approach to fabricating CdSe/ZnS (core/shell) QD micro-ring resonant cavities. The size of the CdSe/ZnS QDs is characterized by the transmission electron microscope (Fig. 1a and Fig. S1). The average diameter of red

QDs and green QDs are 12 nm and 9 nm, respectively, which decides the QD energy band structure and emission wavelength. Figure 1a shows the schematic diagram of the energy band for red CdSe/ZnS QDs. Initially, the hot electron-hole pairs are generated by non-resonant pumping, and then the system emits photons after the relaxation, exciton formation, and recombination. Due to the quantum confinement effects, the exciton will form discrete energy levels and emissions similar to the 1S and 2S states of atoms trapped in a quantum box.

To investigate the discrete excitonic states and radiative recombination process of QDs, we measured the PL spectra for red and green CdSe/ZnS QDs at RT (Fig.1b and Fig. S3). By the fitted PL and absorpance spectrum of red QDs (Fig. S2), one can observe PL emission with two peaks of the center wavelength of 620.5 nm (1.998 eV) and 578.3 nm (2.144 eV), originating from the 1S and 2S state exciton transition, respectively. In power-dependent PL measurements of red QDs (Fig. 1c), the PL spectra show a single peak of 620.5 nm related to the 1S-state transition emission at low pump fluence. With the pumping fluence increasing, the band-filling phenomenon leads to the appearance of 2S state transition and emission (peak of 578.3 nm), owing to the state filling effect of the lowest 1S exciton states, where the increased carrier population gradually occupies higher-energy discrete states. These results indicate that the quantum-confined QDs possess multiple discrete exciton states, providing the possibility of manipulating optical gain through different excitonic transitions. Regarding green QDs, PL and absorption characterizations (Fig. S3) exhibit an exciton emission peak centered at 525.5 nm (2.36 eV) and a strong excitonic absorption centered at 514.5 nm (2.41 eV) at RT. Subsequently, micro-ring arrays of red, green, and blended QDs are fabricated by using customized silicon column templates and solution patterning methods, as shown in Fig. S4. Figure 1d exhibits the ring arrays with great morphological quality and highly uniform ring dimensions. Statistical analysis of the micro-rings in the SEM image gives an average outer diameter of about 12.0 ± 0.4 μm, corresponding to a coefficient of variation of about 3.3%, indicating good dimensional uniformity of the fabricated micro-ring array. Fluorescence

microscopy images (Fig. 1e) show consistent ring-shaped emission patterns for the red, green, and blended QD micro-rings, further demonstrating the uniform optical morphology of the fabricated structures. Thus, we have fabricated high-quality QD ring cavities for subsequent lasing generation.

Lasing characterizations of pure QD micro-rings

After acquiring the high-quality ring resonant cavities, room-temperature lasing phenomena were demonstrated in pure red QD micro-rings with different radii by ultrafast femtosecond pulse laser pumping (400 nm, 1 kHz). Power-dependent PL mapping of the micro ring with a radius of 6 μm is measured and plotted in Fig. 2a. At low-power excitation, the PL peak of red QDs appears at 620.5 nm, corresponding to the spontaneous emission (SE) of 1S exciton transition. With the pump fluence increasing, multiple bright lasing modes appear at 628.1 nm, 632.7 nm, and 638.4 nm at $22\ \mu J\,cm^{-2}$ (1S-state lasing threshold), attributed to the stimulated emission of WGM resonances. Further increasing the excitation density induces population occupation of higher-energy discrete exciton states due to the filling of the 1S exciton states, leading to additional high-energy lasing modes at 582.1 and 586.5 nm. To quantify the lasing behaviors, we analyzed the power-dependent PL intensity and linewidth of the lasing mode of 638.4 nm for 1S-state transition (Fig. 2b), under the pump fluence ranging from $2\ \mu J\,cm^{-2}$ to $101\ \mu J\,cm^{-2}$. The integrated peak intensity as a function of the pump fluence shows a remarkable nonlinear enhancement, surging by nearly two orders of magnitude above the threshold ($22\ \mu J\,cm^{-2}$), which exhibits a typical S-shaped trend. The emission linewidth, extracted from the PL spectrum, decreases from the broad spontaneous emission bandwidth (34.8 nm) below threshold to the narrow WGM lasing linewidth (0.8 nm) above threshold. This sharp linewidth narrowing upon crossing the lasing threshold indicates the formation of coherent WGM lasing, corresponding to a high quality factor (Q factor) of approximately 800. Similarly, the lasing modes originating from the 2S-state transition exhibit comparable Q factors of about 700, suggesting that the cavity quality remains nearly unchanged for different excitonic transitions. The linewidth narrowing and high

Q factor further confirm the formation of coherent WGM lasing emission in QD micro-rings. Although the micro-ring cavity supports WGM resonances, the WGM modes cannot be resolved below threshold due to the insufficient optical gain generated under low pump excitation.

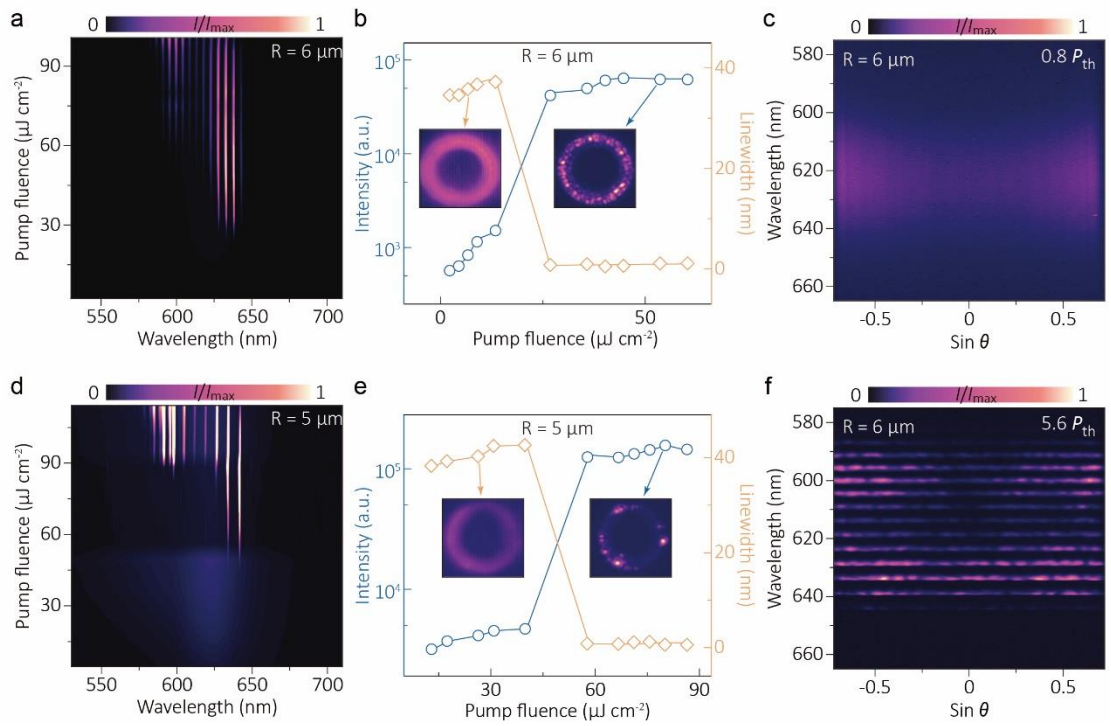


Fig. 2. Lasing for red QD ring resonators with different radii at RT. (a) Power-dependent emission spectra of a red QD ring with a 6 μm radius. (b) PL intensity and linewidth as a function of pump fluence for a 6 μm-radius ring at 638.4 nm, showing the appearance of lasing at $22\ \mu J\,cm^{-2}$. The insets represent real-space images of the ring below and above the threshold, respectively. (c) ARPL spectrum of a 6 μm radius ring below the threshold. (d) Power-dependent emission spectra of a red QD ring with a 5 μm radius. (e) PL intensity and linewidth as a function of pump fluence for a 5 μm radius ring at 634.6 nm, showing the appearance of lasing at $47\ \mu J\,cm^{-2}$. (f) ARPL spectrum of a 6 μm radius ring above the threshold.

Real-space imaging of the red QD micro-ring (the insets of Fig. 2b) provides direct visualization of the spatial evolution of the optical modes during the lasing process. Below the threshold, the QD ring exhibits a uniform doughnut-shaped emission corresponding to SE from the ring. Above the threshold, the real-space emission evolves into a petal-like intensity distribution, reflecting the spatially modulated emission and scattering associated with the WGM lasing modes, despite a few defects

slightly affecting the emission leakage position. Moreover, we measured the angle-resolved PL (ARPL) spectra of red QD rings to investigate the coherence of lasing, as shown in Fig. 2c and 2f (below and above the threshold). ARPL spectrum demonstrates the PL radiates from all angles with a broad bandwidth at $0.8\ P_{\mathrm{th}}$. Above the threshold ($5.6\ P_{\mathrm{th}}$), the ARPL spectrum of the QD micro-ring displays that the interference patterns extend to all emission angles on each lasing mode (Fig. 2f), due to the interference between the same lasing mode emitted from the opposite sides of the micro-ring. These spatial mode distributions and interference patterns confirm that the lasing emission originates from coherent WGM modes supported by the circular micro-ring cavity.

To verify the reproducibility of WGM lasing in QD micro-rings with different cavity dimensions, similar lasing characterizations were performed on red QD micro-rings with a radius of 5 μm, as shown in Fig. 2d and 2e. The lasing behavior is consistent with that observed in the 6 μm micro-ring. Under increasing pump fluence, lasing modes initially emerge around the 1S exciton emission region, followed by additional high-energy modes associated with higher discrete exciton states under strong excitation, resulting from the state-filling effect. Similar nonlinear intensity enhancement, linewidth narrowing, spatial mode evolution, and ARPL interference features are observed for the two micro-ring sizes (Fig. 2e and Fig. S5), confirming the robust WGM lasing characteristics of the QD micro-ring cavities. Furthermore, pure green QD micro-rings were fabricated and investigated as control samples. The pump-dependent PL spectra under excitation fluences ranging from $13\ \mu\mathrm{J\,cm^{-2}}$ to $95\ \mu\mathrm{J\,cm^{-2}}$ are presented in Fig. S6. Above the threshold of $52\ \mu\mathrm{J\,cm^{-2}}$, sharp lasing peaks appear around the low-energy side of the SE peak (525.5 nm), corresponding to the 1S exciton transition. These results indicate that the lasing emission in single-component QD micro-ring resonators is mainly determined by the lowest-energy 1S exciton transition, establishing the intrinsic lasing characteristics of QDs.

Lasing characterizations of blended QD micro-rings

Based on the optical properties and lasing characteristics of pure red and green QDs, we mixed the same concentration of green and red QD solutions in a ratio of 1:1 to obtain a blended QD solution and fabricated the micro-rings with radii of 5 μm and 6 μm. In such micro-rings, the blended QDs form nanoscale heterojunctions due to the bandgap difference between red and green QDs, providing additional exciton transfer pathways compared with single-component QDs. To investigate the effect of band heterostructures on the lasing, we measured the lasing performance of blended QD micro-rings at RT by the femtosecond pulsed laser excitation. Figure 3a shows the power-dependent PL spectra mapping of the micro-ring with a radius of 6 μm. At low pump power, two broad PL peaks are located at 620.5 nm and 525.5 nm with broad linewidth, which originates from SE of the 1S state transition for red (acceptor) and green (donor) parts in blended QDs, respectively, indicating that both QDs retain their intrinsic excitonic emission characteristics in the blended system. When the pump fluence increases to $17.1\ \mu J\,cm^{-2}$, multiple narrow lasing peaks appeared in the PL mapping at 578.8 nm, 582.6 nm, and 586.5 nm, corresponding to the stimulated emission from the 2S exciton transition of red QDs. Notably, lasing emissions appear first on the SE peak of the 2S state instead of the 1S state, which is distinct from the 1S-state-dominated lasing observed in pure QD micro-rings. As the further increase of pump fluence, additional high-energy lasing modes appear such as 561.6 nm, 565.1 nm, and 568.4 nm (Fig. 3b). The lasing performance is characterized by the power-dependent intensity and linewidth for the mode of 586.5 nm, under the pump fluence ranging from $0.8\ \mu J\,cm^{-2}$ to $48.6\ \mu J\,cm^{-2}$, as shown in Fig. 3c. A pronounced nonlinear increase in emission intensity spans two orders of magnitude and the linewidth sharply shrinks from 35.1 nm to 0.5 nm above the threshold, corresponding to a high Q factor of approximately 1170. The insets of Fig. 3c show real-space images of the SE and lasing emissions with a doughnut-shaped and petal-like emission pattern, respectively. Angle-resolved PL spectra still demonstrate the lasing interference fringes at $2.3\ P_{th}$ (Fig. S7). Similar spatially modulated emission patterns and ARPL interference fringes further confirm the WGM nature of the lasing modes in blended QD micro-rings.

To further verify the reproducibility of the 2S-state lasing behavior, blended QD micro-rings with a radius of 5 μm were also investigated. Similar to the case of 6 μm radius, the micro-ring undergoes a transition from SE to lasing emission as the pump fluence increases from $5.3\ \mu J\ cm^{-2}$ to $73.3\ \mu J\ cm^{-2}$ (Fig. 3d). Above the threshold, the lasing peaks appear at the 2S-state, such as 580.8 nm, 584.5 nm, and 588.4 nm (Fig. 3e). The intensity, linewidth, and real-space images show nonlinear enhancement, shrinking, and spatially modulated emission patterns, respectively, with pump fluence increasing (Fig. 3f). The lasing modes exhibit Q factors of approximately 800, comparable to those obtained from the 6 μm-radius blended QD micro-rings. These results further verify that the lasing emission in blended QD micro-rings preferentially originates from the 2S exciton transition.

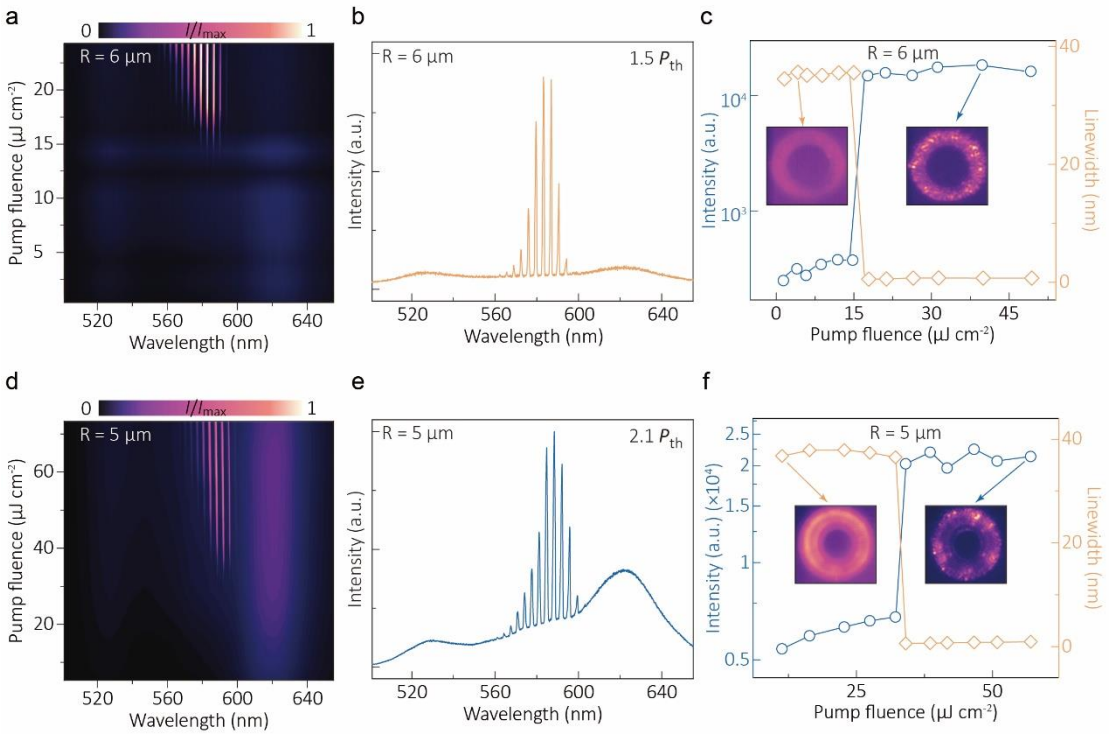


Fig. 3. Lasing from blended QD ring resonators with different radii at RT. (a) Power-dependent mapping of the emission spectra of a 6 μm-radius blended QD ring. (b) PL spectra of a 6 μm-radius ring above the threshold at $1.5\ P_{th}$. (c) PL intensity and linewidth as a function of pump fluence for a 6 μm-radius ring at 586.5 nm, showing the appearance of lasing at $17.1\ \mu J\ cm^{-2}$. The insets represent real-space images of the ring below and above the threshold, respectively. (d) Power-dependent emission spectra of a 5 μm-radius blended QD ring. (e) PL spectra of a 5 μm-radius ring above the threshold at $2.1\ P_{th}$. (f) PL intensity and linewidth as a function of pump fluence for a 5 μm-radius ring at 592.6 nm, showing the

appearance of lasing at $33\ \mu J\ cm^{-2}$.

Mechanisms of lasing in blended QD micro-rings

To elucidate the origin of the 2S-state lasing emission and the exciton population redistribution in blended QD micro-rings, we depicted a hetero-band structure for blended QD within micro-rings, as shown in Fig. 4a. Once blended QDs are fabricated as a micro-ring, red and green QDs are closely aligned and form a type-I heterojunctions. Due to the larger bandgap of green QDs compared with red QDs, the spectral overlap between donor (green QDs) emission and acceptor (red QDs) absorption enables FRET from green donor QDs to red acceptor QDs. When the blended QD micro-ring is nonresonantly excited, electrons and holes are initially generated in red and green QDs and then form excitons, subsequently relaxing to lower energy levels. Regarding the donor (green QDs) of the blend, the excitons are relaxed to the 1S state and get radiate recombination, while part of them are resonantly transferred to excited states of acceptors (red QDs) through FRET due to the spectral overlap between donor emission and acceptor absorption. The transferred excitons contribute to the excited-state population of acceptor (red QDs) and modify the population distribution among different exciton states. Regarding the acceptor (red QDs), excitons can relax through the 2S and 1S exciton states. At the same time, the 2S state of acceptors also gains excitons from the donors through the FRET process. As a result, the exciton accumulation on the 2S state of acceptors is larger than the accumulation on the 1S state of both acceptors and donors, and population inversion can be eventually achieved to produce lasing on the 2S state. Consequently, optical gain is preferentially established on the 2S exciton transition, enabling 2S-state lasing in blended QD micro-rings, while the strong absorption and relaxation losses of the 1S state prevent preferential lasing from this transition. In contrast, excitons in pure red or green QDs mainly relax toward the lowest-energy 1S state without inter-QD energy transfer pathways, resulting in conventional 1S-state-dominated lasing. The different lasing transitions between blended and pure QD micro-rings are consistent with the experimental spectra shown in Fig. 4b and Fig. S8.

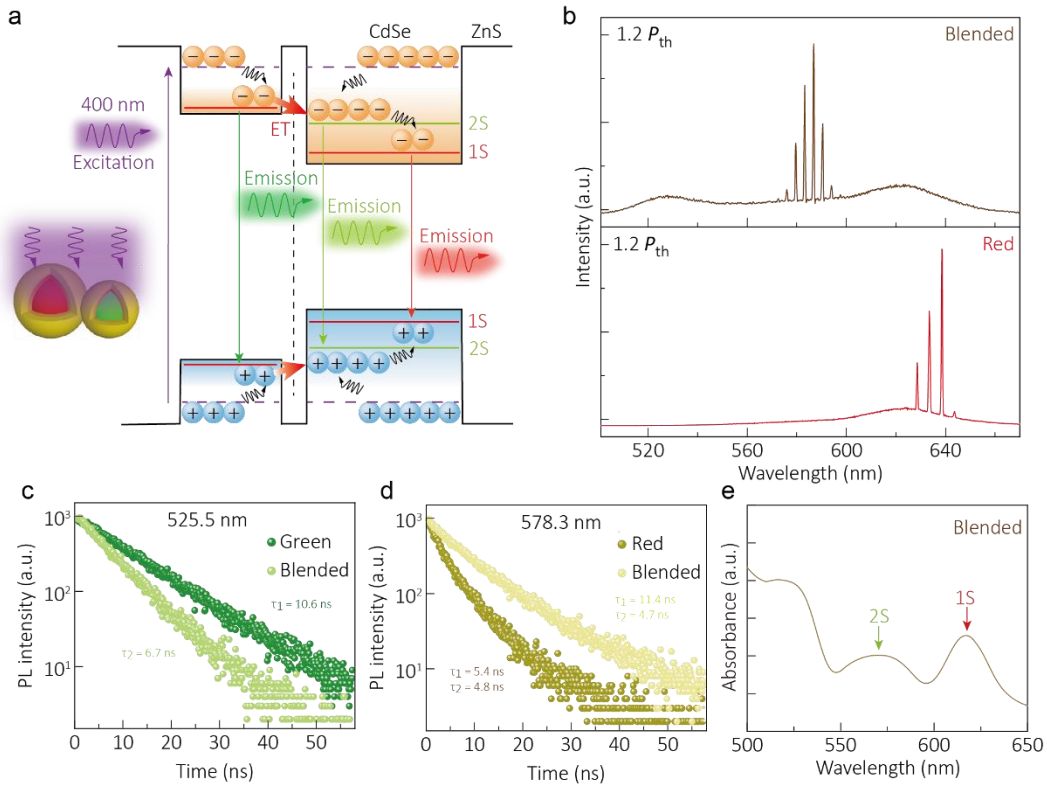


Fig. 4. Comparison and analysis of lasing for red and blended QD rings. (a) Schematic diagram of PL of blended QD ring resonators. (b) PL spectra of red and blended QD ring resonators with a radius of 6 μm above the threshold at 1.2 P_{th}. (c) PL dynamics for 1S state at 525.5 nm of green QDs (Dark green) and blended QDs (light green). (d) PL dynamics for 2S state at 578.3 nm of red QDs (brown) and blended QDs (yellow). (e) Absorption of blended QDs at RT. The red and green arrows refer to the 1S and 2S states of the acceptor parts, respectively.

To experimentally verify the exciton dynamics with a FRET process in blended QDs, time-resolved PL (TRPL) measurements were performed on pure and blended QDs, followed by PL lifetime analysis. Regarding the donor state (1S state of green QDs, 525.5 nm), the PL lifetime decreases from 10.6 ns in pure green QDs to 6.7 ns in blended QDs, as shown in Fig. 4c. The reduced lifetime after blending indicates the existence of an additional energy transfer pathway from donor to acceptor QDs. Based on the donor lifetime variation, the FRET efficiency is calculated to be 36.8%, corresponding to a FRET transfer rate of $5.5 \times 10^7\ s^{-1}$ (see Supplementary Information). This quantitative analysis confirms the effective exciton transfer from green donor QDs to red acceptor QDs. Regarding the acceptor states (2S state of red QDs, 578.3 nm), pure red QDs exhibit a single-exponential decay with a lifetime of 3.8

ns (Fig. 4d), corresponding to SE from the 2S exciton transition. In contrast, blended QDs show a biexponential decay with lifetime components of 11.4 and 4.7 ns, indicating modified exciton relaxation dynamics after introducing donor QDs. Compared with pure red QDs, the prolonged 2S-state lifetime in blended QDs suggests modified exciton population dynamics and relaxation pathways after introducing donor QDs. Moreover, the absorption spectrum of blended QDs was analyzed to investigate the optical competition between gain and loss for the 1S and 2S exciton states (Fig. 4e). Although the 1S transition possesses a stronger oscillator strength and can provide optical gain, the simultaneously enhanced ground-state absorption introduces considerable reabsorption loss, resulting in an unfavorable gain-loss balance. In contrast, the 2S transition exhibits reduced absorption loss and benefits from the FRET-mediated exciton redistribution, leading to a more favorable gain-loss condition under high excitation densities. Therefore, the lasing wavelength is determined by the balance between optical gain and loss rather than absorption intensity alone. The quantitative analysis based on the absorption spectra (see Supplementary Information) further confirms that the 2S transition exhibits a more favorable gain-loss condition than the 1S transition, facilitating preferential lasing emission from the 2S transition. Combined with the FRET-mediated exciton redistribution, which promotes exciton accumulation in the acceptor 2S state, the blended QD micro-rings therefore achieve 2S-state lasing rather than the conventional 1S-state lasing observed in single-component QD systems. Different from previous studies in which state filling or FRET was mainly associated with excited-state emission, optical-gain enhancement, or improved lasing performance[12,18], the present results show that FRET-mediated exciton redistribution, together with band filling and state-dependent gain–loss competition, can regulate the preferential lasing exciton state.

Conclusion

In summary, we have fabricated high-quality and uniform micro-ring resonators with pure and blended QDs using the solution self-assembled patterning method and realized WGM lasing emission in them at RT. The steady-state PL spectra demonstrate

the 1S and 2S exciton transitions in pure red QDs and reveal the band-filling effect under high excitation density. The power-dependent PL experiments further confirm that pure red QD micro-rings exhibit lasing emission originating from the 1S exciton state. Based on the results, we further blended the red and green QDs to construct heterojunctions on the nanoscale. In the blended QD rings, lasing emission occurs preferentially from the 2S exciton state, which is distinct from the 1S-state lasing observed in pure QD rings. To explain the phenomenon, we propose a transition model and reveal that FRET-mediated exciton transfer, together with state-dependent gain-loss competition, regulates exciton redistribution and improves the gain-loss condition of the 2S state, thereby enabling population inversion and preferential 2S-state lasing emission. These findings demonstrate the capability of QD composition engineering to manipulate exciton dynamics and lasing transitions, providing a feasible strategy for developing tunable on-chip QD microcavity lasers and optoelectronic devices.

Supporting Information

See Supplementary Information for supporting content.

Acknowledgments

The authors gratefully acknowledge the financial support from National Key Research and Development Program of China (2023YFA1407100) and National Natural Science Foundation (12574412).

References

[1] García de Arquer F P, Talapin D V, Klimov V I, Arakawa Y, Bayer M and Sargent E H 2021 *Science* **373** eaaz8541.

[2] Park Y-S, Roh J, Diroll B T, Schaller R D and Klimov V I 2021 *Nat. Rev. Mater.* **6** 382.

[3] Rossetti R, Nakahara S and Brus L E 1983 *J. Chem. Phys.* **79** 1086.

[4] Alivisatos A P 1996 *Science* **271** 933.

[5] Murray C B, Norris D J and Bawendi M G 2002 *J. Am. Chem. Soc.* **115** 8706.

[6] Moreels I, Lambert K, Smeets D, De Muynck D, Nollet T, Martins J C, Vanhaecke F, Vantomme A, Delerue C, Allan G and Hens Z 2009 *ACS Nano* **3** 3023.

[7] Empedocles S A and Bawendi M G 1997 *Science* **278** 2114.

[8] Weidman M C, Beck M E, Hoffman R S, Prins F and Tisdale W A 2014 *ACS Nano* **8** 6363.

[9] Hanifi D A, Bronstein N D, Koscher B A, Nett Z, Swabeck J K, Takano K, Schwartzberg A M, Maserati L, Vandewal K, van de Burgt Y, Salleo A and Alivisatos A P 2019 *Science* **363** 1199.

[10] Fan F, Voznyy O, Sabatini R P, Bicanic K T, Adachi M M, McBride J R, Reid K R, Park Y-S, Li X, Jain A, Quintero-Bermudez R, Saravanapavanantham M, Liu M, Korkusinski M, Hawrylak P, Klimov V I, Rosenthal S J, Hoogland S and Sargent E H 2017 *Nature* **544** 75.
[11] Klimov V, Mikhailovsky A, Xu S, Malko A, Hollingsworth J, Leatherdale C, Eisler H and Bawendi M 2000 *Science* **290** 314.
[12] Ahn N, Livache C, Pinchetti V and Klimov V 2023 *Chem. Rev.* **123** 8251.
[13] Ahn N, Livache C, Pinchetti V, Jung H, Jin H, Hahm D, Park Y-S and Klimov V I 2023 *Nature* **617** 79.
[14] le Feber B, Prins F, De Leo E, Rabouw F T and Norris D J 2018 *Nano Lett.* **18** 1028.
[15] Zeng Q, Lafalce E, Lin C H, Smith M J, Jung J, Yoon Y, Lin Z, Tsukruk V V and Vardeny Z V 2019 *Nano Lett.* **19** 6049.
[16] Wang Y, Ta V D, Leck K S, Tan B H I, Wang Z, He T, Ohl C-D, Demir H V and Sun H 2017 *Nano lett.* **17** 2640.
[17] Geuchies J J, Brynjarsson B, Grimaldi G, Gudjonsdottir S, Van Der Stam W, Evers W H and Houtepen A J 2021 *ACS nano* **15** 377.
[18] Song Z, Lei H, Zhu Y, Lin X and Peng X 2026 *ACS Photonics* **13** 1734.
[19] Talapin D V, Mekis I, Götzinger S, Kornowski A, Benson O and Weller H 2004 *J. Phys. Chem. B* **108** 18826.
[20] Cragg G E and Efros A L 2010 *Nano Lett.* **10** 313.
[21] Chen O, Zhao J, Chauhan V P, Cui J, Wong C, Harris D K, Wei H, Han H-S, Fukumura D, Jain R K and Bawendi M G 2013 *Nat. Mater.* **12** 445.
[22] Coropceanu I and Bawendi M G 2014 *Nano Lett.* **14** 4097.
[23] Hines M A and Guyot-Sionnest P 1996 *J. Phys. Chem.***100** 468.
[24] Wang Z, Lenngren N, Amarotti E, Hedse A, Zídek K, Zheng K, Zigmantas D and Pullerits T 2022 *J. Phys. Chem. Lett.* **13** 1266.
[25] Sousa Velosa F, Van Avermaet H, Schiettecatte P, Mingabudinova L, Geiregat P and Hens Z 2022 *Adv. Opt. Mater.* **10** 14.
[26] Li X, Du J, Zhao G, Zhang B, Livache C, Ahn N, Jia Y, Li M, Chen Y and Zhu J 2024 *Adv. Mater.* **36** 2308979.
[27] Park Y-S, Bae W K, Baker T, Lim J and Klimov V I 2015 *Nano Lett.* **15** 7319.
[28] Pang Z, Zhang J, Cao W, Kong X and Peng X 2019 *Nat. Commun.* **10** 2454.
[29] McGranahan C R, Wolfe G E, II, Falca A and Watson D F 2021 *ACS Appl. Mater. Interfaces* **13** 30980.
[30] Chern M, Toufanian R and Dennis A M 2020 *Analyst* **145** 5754.
[31] Montanarella F, Biondi M, Hinterding S, Vanmaekelbergh D and Rabouw F 2018 *Nano Lett.* **18** 5867.
[32] Chou K and Dennis A 2015 *Sensors* **15** 13288.
[33] Lee T C, Lin H Y, Tsao Y C, Lu G Z, Hsieh Y-P and Chen Y F 2025 *Nanoscale* **17** 23511.
[34] Shen T-L, Hu H-W, Lin W-J, Liao Y-M, Chen T-P, Liao Y-K, Lin T-Y and Chen Y-F 2020 *Sci. Adv.* **6** eaba1705.
[35] Dusanowski Ł, Köck D, Shin E, Kwon S-H, Schneider C and Höfling S 2020 *Nano Lett.***20** 6357.
[36] Montanarella F, Urbonas D, Chadwick L, Moerman P G, Baesjou P J, Mahrt R F, Van Blaaderen A, Stoferle T and Vanmaekelbergh D 2018 *ACS nano* **12** 12788.
[37] Wang J, Xu H, Su R, Peng Y, Wu J, Liew T C H and Xiong Q 2021 Light: Science & Applications

10 45.
[38] Feng J, Gong C, Gao H, Wen W, Gong Y, Jiang X, Zhang B, Wu Y, Wu Y, Fu H, Jiang L and Zhang X 2018 *Nat. Electron.* **1** 404.

Supplementary Information

Room Temperature Lasing in Micro-Rings of Blended Core/Shell Quantum Dots

Zehua Ren（任则华）[1,#], Xiaoyu Wang（王小宇）[1,#], Zelei Chen（陈泽磊）[1], Dachuan Li（李大川）[1], Zhongmin Huang（黄钟民）[1], Gang Ni（倪刚）[1], Chuanxiang Sheng（盛传祥）[1,2], Jun Wang（王俊）[1,2,*]

[1] Key Laboratory of Micro & Nano Photonic Structures, Department of Optical Science and Engineering, College of Future Information Technology, Fudan University, Shanghai, 200433, China

[2] State Key Laboratory of Photovoltaic Science and Technology, Shanghai Key Laboratory of Metasurfaces for Light Manipulation, Fudan University, Shanghai, 200433, China

[#] *These authors contributed equally to this work.*

[*] Corresponding to: wangjunfd@fudan.edu.cn; wuyuchen@iccas.ac.cn

Keywords: photonic lasing, microcavity, colloidal quantum dots, solution patterning method

This file includes:

1. Morphology characterization of red and green CdSe/ZnS quantum dots (QDs) (Fig. S1)
2. Absorption spectra of red CdSe/ZnS QDs
3. Absorption and PL spectra of green CdSe/ZnS QDs (Fig. S3)
4. Fabrication of QD micro-rings (Fig. S4)
5. Lasing and angle-resolved PL spectra of red QD micro-rings with different radii (Fig. S5)
6. Characterization of lasing from green QD micro-rings (Fig. S6)
7. Angle-resolved PL spectrum of the blended QD micro-ring (Fig. S7)
8. Estimation of WGM mode orders from resonance spacing
9. Comparison of PL spectra for red and blended QD micro-rings with different radii (Fig. S8)
10. Quantitative evaluation of Förster resonance energy transfer
11. Exciton population dynamic model
12. Gain-loss analysis between 1S and 2S transitions
13. Influence of Auger recombination on exciton population

1. Morphology characterization of red and green CdSe/ZnS quantum dots (QDs)

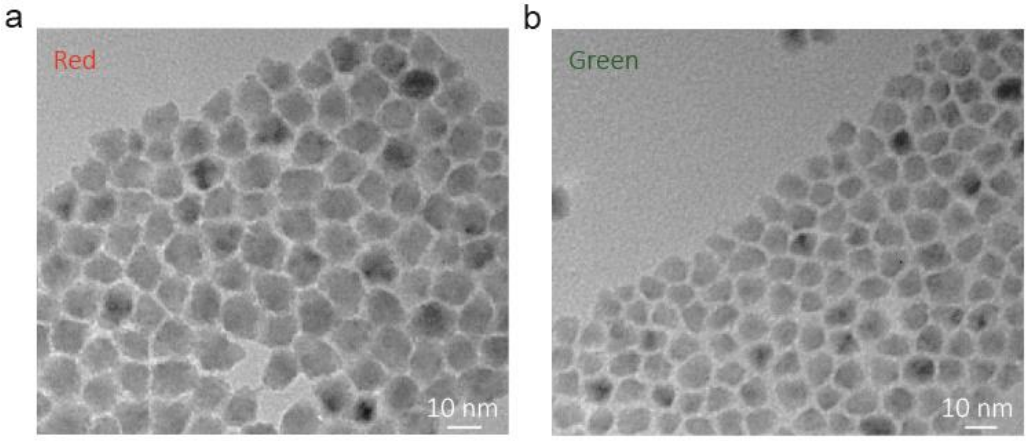


Figure S1. Transmission electron microscope (TEM) image of red (left) and green (right) QDs. The mean diameter of red and green QDs is 12 nm and 9 nm, respectively.

2. Absorption spectra of red CdSe/ZnS QDs

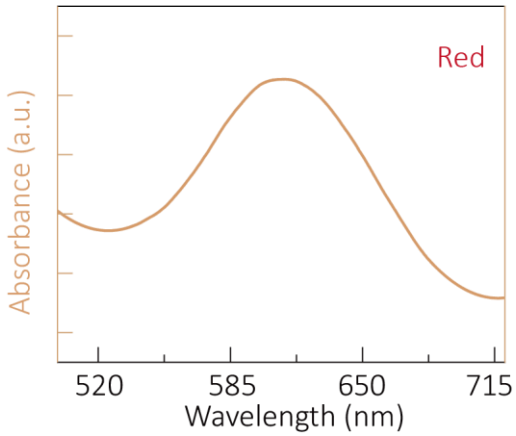


Figure S2. Absorption spectra of red CdSe/ZnS QDs at room temperature. Absorption spectrum shows a strong excitonic absorption centered at 610.5 nm.

3. Absorption and PL spectra of green CdSe/ZnS QDs

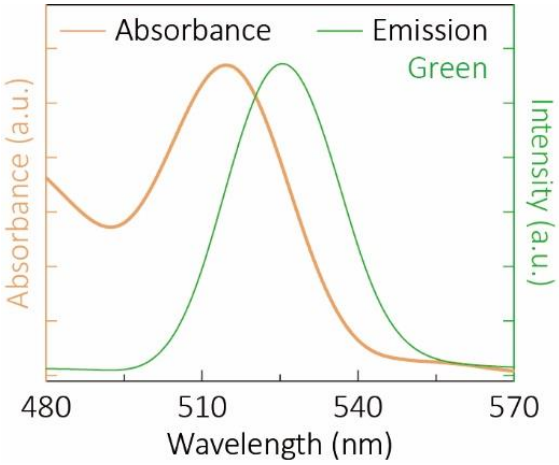


Figure S3. Absorption (orange) and PL (green) spectra of green CdSe/ZnS QDs at room temperature. PL spectrum exhibits an exciton emission peak centered at 525.5 nm with a linewidth of 26.5 nm and the absorption spectrum shows a strong excitonic absorption centered at 514.5 nm.

4. Fabrication of QD micro-rings

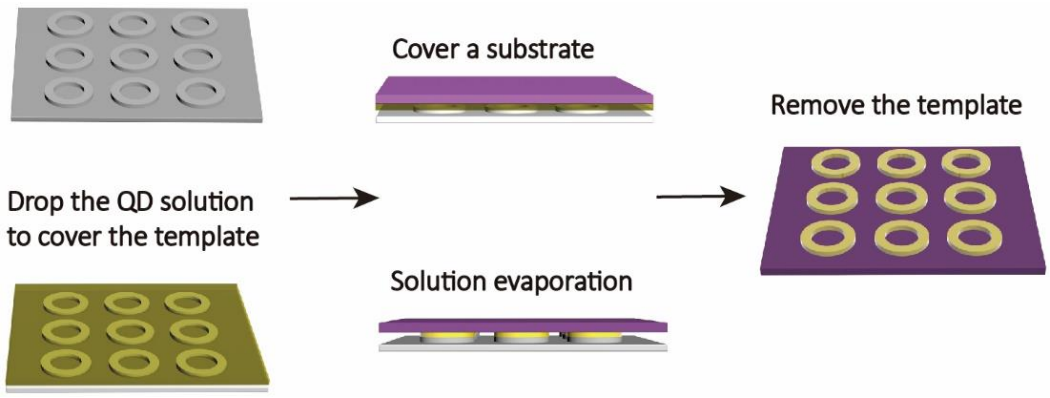


Figure S4. Fabrication of QD micro rings and the dewetting process. Schematic illustration of the method for fabrication of QD micro-rings. A precise amount of QD solution is dropped on the template and then covered with the target substrate. After the solution fully evaporates, the template is removed, leaving an array of QD micro-rings.

5. Lasing and angle-resolved PL spectra of red QD micro-rings with different radii

We measured PL spectra of red QD micro-ring lasers with a radius of 6 μm (Fig. S5a) and a radius of 5 μm (Fig. S5b) above the threshold. At the high pump power, a series of sharp lasing peaks appear on the spontaneous emission (SE) spectrum of 620.5 nm and 578.3 nm, corresponding to 1S and 2S exciton transition. Due to the resonant mode number dependent on the radius, the ring with a radius of 5 μm has fewer lasing modes. The Q factors of the 1S- and 2S-state lasing peaks are about 800 and 700, respectively. The angle-resolved PL spectrum of a red QD ring with a radius of 5 μm is measured to prove the establishment of lasing coherence (Fig. S5c and S5d).

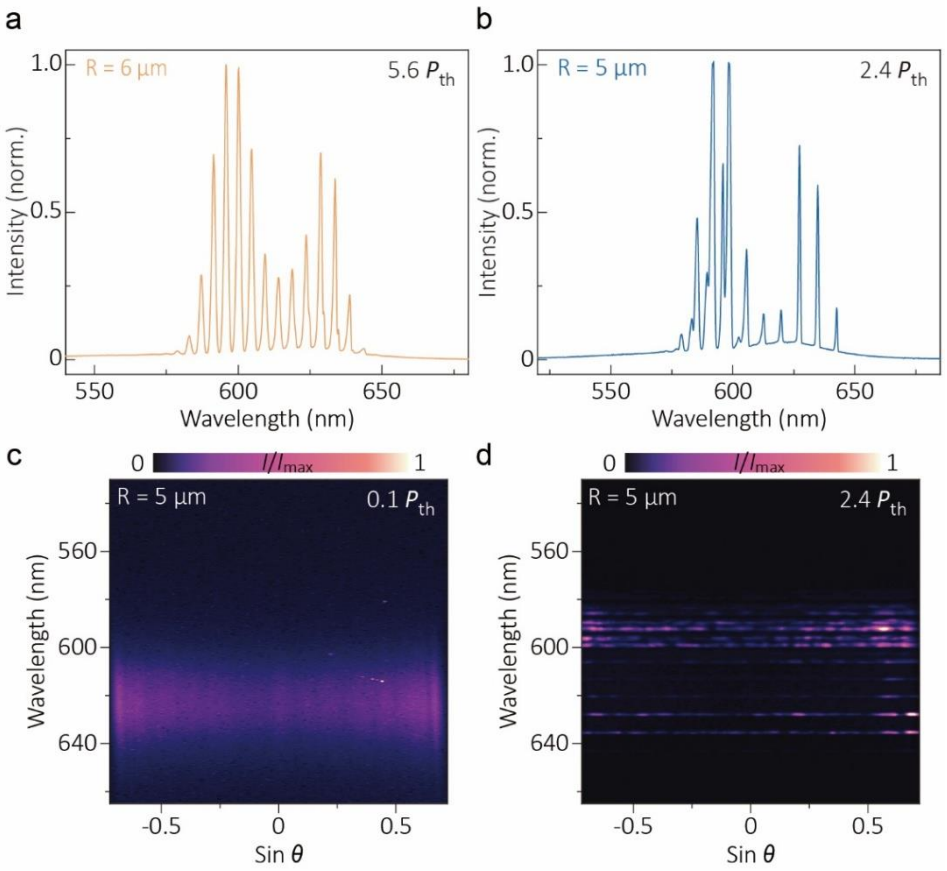


Figure S5. Characterizations of lasing for red QD micro rings with different radii at room temperature. (a) PL spectra of the red QD ring with 6 μm radius above the threshold, referred to Fig. 2a of the main text. (b) PL spectra of the red QD ring with 5 μm radius above the threshold, referred to Fig. 2d of the main text. (c) Angle-resolved PL spectrum of the red QD ring with 5 μm radius below the threshold. (d) Angle-resolved PL spectrum of the red QD ring with 5 μm radius above the threshold.

6. Characterization of lasing from green QD micro-rings

The micro rings of pure green CdSe/ZnS QDs exhibit lasing phenomena similar to those of the pure red QD micro-rings. The laser peaks appear on the 1S-state SE spectrum of 525.5 nm (Fig. S6a), with Q factors of approximately 780. The intensity of these laser peaks increases with the pump fluence rising (Fig. S6b).

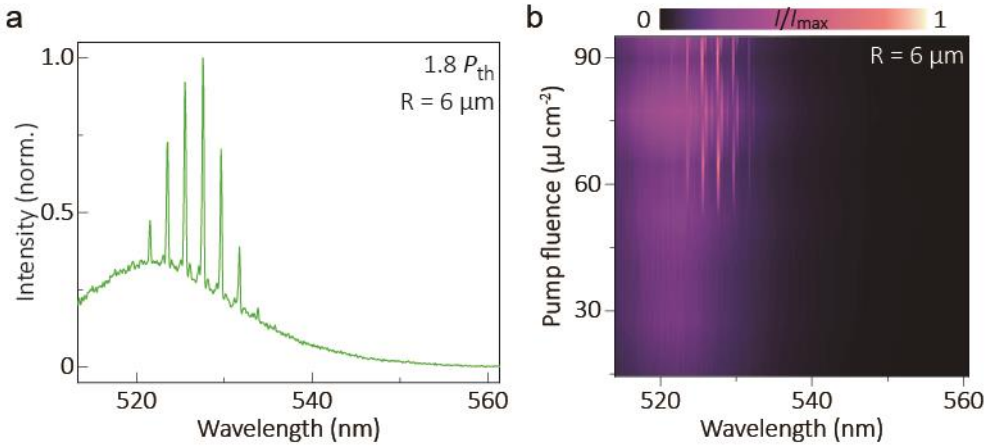


Figure S6. Characterization of lasing from green QD micro-ring with a radius of 6 μm at room temperature. (a) PL spectrum of a green QD ring above the threshold at $1.8\ P_{th}$. (b) Power-dependent PL spectra of a 6 μm radius green QD ring with pump fluence increasing from $13\ \mu J\ cm^{-2}$ to $95\ \mu J\ cm^{-2}$. The lasing threshold is $52\ \mu J\ cm^{-2}$.

7. Angle-resolved PL spectrum of the blended QD micro-ring

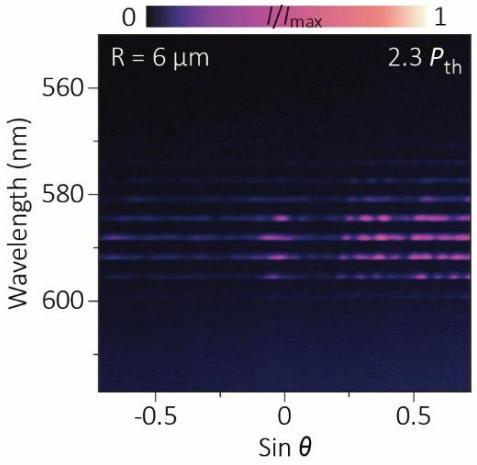


Figure S7. Angle-resolved PL spectrum of the blended QD ring with a 6 μm radius above the threshold at $2.3\ P_{th}$, corresponding to Fig. 3b of the main text.

8. Estimation of WGM mode orders from resonance spacing

To further analyze the cavity mode characteristics of the QD micro-ring lasers, the WGM orders were estimated based on the resonance spacing of the lasing modes. For a ring resonator, the resonance condition of WGM can be approximately described as[1]:

$$m\lambda = 2\pi n_{\mathrm{eff}} R$$

where mr epresents the azimuthal mode number, n_{eff} is the effective refractive index, R is the radius of the micro-ring cavity, and λ is the resonance wavelength. For adjacent azimuthal modes, the mode order can be approximately estimated from the free spectral range:

$$m \approx \frac{\lambda}{\Delta\lambda}$$

where $\Delta\lambda$ represents the wavelength spacing between adjacent resonance modes.

For the pure red QD micro-ring, multiple discrete resonance peaks are observed around the 1S exciton emission region. According to the resonance wavelength and the mode spacing extracted from the spectrum, the corresponding azimuthal mode number is estimated to be about 123. Similarly, the blended QD micro-ring exhibits discrete resonance peaks in the 2S exciton emission region, and the estimated azimuthal mode number is about 151. The comparable high-order mode numbers indicate that the lasing emissions from both pure red and blended QD micro-rings originate from high-order WGM resonances supported by the micro-ring cavities.

Together with the angle-dependent resonance features observed in the ARPL measurements and the ring-shaped spatial emission distributions, the estimated WGM mode orders further confirm the cavity-mode characteristics of the lasing emission. These results demonstrate that the FRET-mediated exciton redistribution in blended QD micro-rings changes the preferred lasing transition from the 1S state to the 2S state, while the underlying WGM cavity mechanism remains unchanged.

9. Comparison of PL spectra for red and blended QD micro-rings with different radii

To better present the difference in lasing emission between the blended and pure QD micro-rings, we measured their PL spectra with different radii above the threshold. The lasing peaks of the pure red QD rings appear on the 1S-state transition spectrum (Fig. S8a), while the lasing peaks of the blend appear on the 2S-state transition spectrum of acceptors (Fig. S8b).

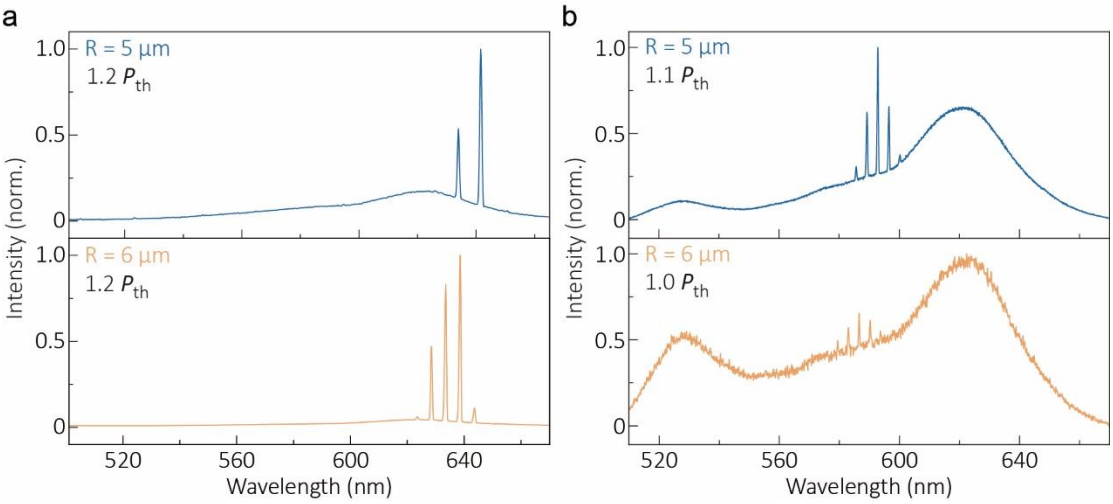


Figure S8. Comparison of PL spectra for red and blended QD micro-rings with different radii above the threshold. (a) Lasing spectra of pure red QD rings with a 5 μm (blue) and a 6 μm(orange) radius at 1.2 P_{th}. (b) Lasing spectra of blended QD rings with a 5 μm (blue) and a 6 μm (orange) radius above the threshold.

10. Quantitative evaluation of Förster resonance energy transfer

To quantitatively verify the exciton transfer process between green donor QDs and red acceptor QDs, time-resolved photoluminescence (TRPL) measurements were performed for pure green QDs and green/red blended QDs. For pure green QDs, the obtained lifetime τ_D represents the intrinsic exciton recombination process of donor QDs. After blending with red QDs, the shortened lifetime τ_{DA} originates from the additional nonradiative energy transfer channel between donor and acceptor QDs. The FRET efficiency was calculated as[2]:

$$E_{FRET} = 1 - \frac{\tau_{DA}}{\tau_D}$$

where E_{FRET} represents the fraction of donor excitons transferred to acceptor QDs through the FRET process. Based on the measured donor lifetimes of pure green QDs and blended QDs, the FRET efficiency was determined to be 36.8%, indicating that a considerable fraction of excitons in donor QDs can be transferred to acceptor QDs through the FRET pathway.

Furthermore, the FRET transfer rate was obtained from:

$$k_{FRET} = \frac{1}{\tau_{DA}} - \frac{1}{\tau_D}$$

The calculated k_{FRET} is $5.5 \times 10^7\ \mathrm{s}^{-1}$, which is comparable to the intrinsic donor recombination rate ($k_D = 9.4 \times 10^7\ \mathrm{s}^{-1}$). This result demonstrates that FRET acts as an effective competing exciton relaxation channel in the blended QDs[3].

To further estimate the spatial coupling between donor and acceptor QDs, the Förster radius R_0 can be related to the spectral overlap between donor emission and acceptor absorption as:

$$R_0^6 = 8.79 \times 10^{-25} \kappa^2 n^{-4} \Phi_D J$$

where κ^2 is the orientation factor, n is the refractive index of the surrounding medium, Φ_D is the donor quantum yield, and J is the spectral overlap integral.

The donor–acceptor distance r is related to the FRET efficiency through:

$$E_{FRET} = \frac{1}{1 + (\frac{r}{R_0})^6}$$

By considering randomly oriented QD dipoles, the ligand environment of colloidal CdSe/ZnS QDs, and the spectral overlap between donor emission and acceptor absorption spectra, the Förster coupling condition was further evaluated. The calculated spectral overlap indicates sufficient interaction between the green donor emission and red acceptor absorption, providing the prerequisite for efficient FRET. According to the experimentally obtained FRET efficiency (36.8%), the donor–acceptor separation is estimated to be comparable to the Förster radius, suggesting that the blended CdSe/ZnS QDs are located within the effective distance range for Förster resonance energy transfer.

These quantitative analyses demonstrate that exciton transfer from green donor QDs to red acceptor QDs is an efficient relaxation pathway in the blended system. The extracted FRET efficiency, transfer rate, and spatial coupling condition collectively support the proposed FRET-assisted exciton injection mechanism responsible for the population redistribution and accumulation at the acceptor states.

11. Exciton population dynamic model

To quantitatively understand the transition from sequential 1S/2S-state lasing in pure red QD micro-rings to preferential 2S-state lasing in blended QD micro-rings, an exciton population dynamics model was established by considering the competition between exciton generation, FRET-mediated energy transfer, and intra-dot exciton relaxation[2-4]. The evolution of exciton populations in donor and acceptor QDs can be described by the following rate equations:

$$\frac{dN_D}{dt} = G_D - (k_D + k_{FRET})N_D$$

$$\frac{dN_{2S}}{dt} = k_{FRET}N_D + G_{2S} - (k_{2S} + k_{rel})N_{2S}$$

$$\frac{dN_{1S}}{dt} = G_{1S} + k_{rel}N_{2S} - k_{1S}N_{1S}$$

where N_D, N_{2S}, and N_{1S} represent the exciton populations in donor QDs, acceptor 2S exciton states, and acceptor 1S exciton states, respectively. G_D, G_{2S}, and G_{1S} represent the photoexcitation-induced exciton generation rates. k_{FRET} denotes the exciton transfer rate from

donor QDs to the acceptor 2S exciton state, while k_{rel} describes the intra-dot relaxation process from the 2S to 1S exciton state. The decay rates k_D, k_{2S}, and k_{1S} describe the corresponding exciton recombination processes.

For pure red QD micro-rings, $k_{FRET} = 0$ due to the absence of donor QDs. Under optical excitation, exciton populations are distributed among different confined states, while the higher-energy 2S excitons undergo intra-dot relaxation toward the 1S exciton state. Therefore, the 1S exciton transition achieves a more favorable population condition and reaches lasing first, consistent with the experimentally observed 1S-state lasing. With increasing pump fluence, state filling gradually enhances the population of higher-energy states, enabling the emergence of subsequent 2S-state lasing.

For blended QD micro-rings, green QDs introduce an additional FRET-mediated exciton injection pathway into the red-QD 2S exciton state. The effective generation rate of acceptor 2S excitons can therefore be expressed as:

$$G_{2S}^{eff} = G_{2S} + k_{FRET} N_D$$

The additional FRET feeding enhances the relative population of the 2S exciton state compared with the 1S state. Combined with the lower absorption loss of the 2S transition, this population redistribution provides a favorable gain-loss condition and contributes to the preferential realization of 2S-state lasing in blended QD micro-rings.

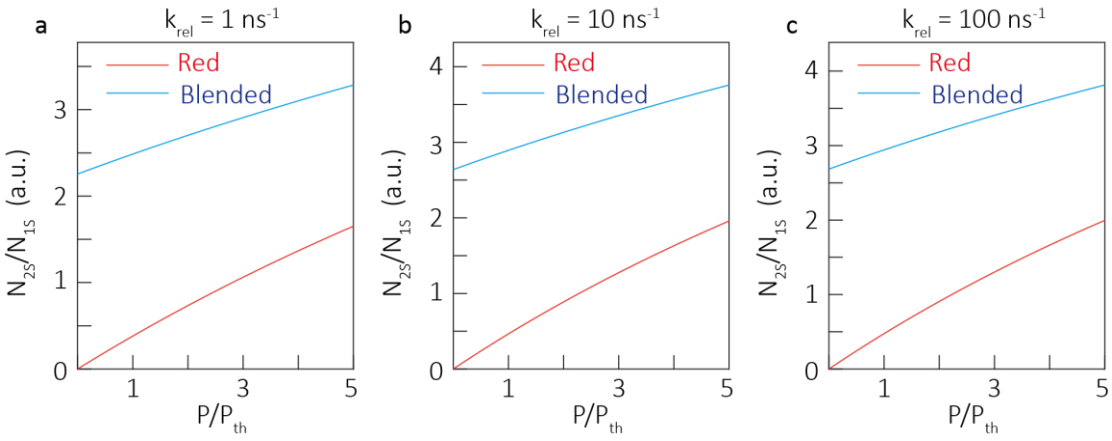


Figure S9. Rate-equation simulation of the exciton population ratio versus normalized pump fluence for pure red and blended QDs with different intraband relaxation rates. (a) 1 ns^{-1}, (b) 10 ns^{-1}, and (c) 100 ns^{-1}.

12. Gain-loss analysis between 1S and 2S transitions

To understand the preferential 2S-state lasing in blended QD micro-rings, the gain-loss competition between the 1S and 2S exciton transitions was analyzed. The lasing threshold is determined by the balance between optical gain and optical loss[4]:

$$\Gamma g(\lambda) > \alpha_{loss}$$

where $g(\lambda)$ represents the optical gain, Γ is the confinement factor, and α_{loss} represents the total optical loss.

Since exciton population is an important factor determining the optical gain, the relative exciton population distribution between the 1S and 2S states was evaluated using the rate-equation model. The calculated N_{2S}/N_{1S} ratio increases in blended QDs due to FRET-mediated exciton transfer, indicating a favorable population condition for the 2S transition. Although the absolute value depends on k_{rel}, the enhancement trend remains unchanged. The absorption-related loss was further evaluated by comparing the integrated absorption intensities of the 1S and 2S transitions. The estimated integrated absorption intensity ratio is $\alpha_{1S}/\alpha_{2S} \approx 1.4$, indicating stronger absorption-related loss for the 1S transition than the 2S transition. These results quantitatively support that the FRET-induced favorable exciton population redistribution and reduced absorption-related loss jointly contribute to the preferential 2S-state lasing.

13. Influence of Auger recombination on exciton population

In colloidal semiconductor QDs, Auger recombination is an important many-body process that influences exciton population dynamics under high excitation densities. When multiple excitons are generated within a single QD, Auger recombination introduces an additional nonradiative decay pathway, which reduces the available exciton population and limits the achievable optical gain[5].

In pure QD systems, increasing pump fluence can induce multiexciton generation and enhance Auger-related losses, thereby restricting further exciton accumulation and optical amplification. In the blended QD heterostructure, FRET provides an additional exciton transfer pathway from donor QDs to acceptor QDs, shortening the donor exciton lifetime and modifying the competition between exciton transfer, multiexciton accumulation, and Auger recombination. Meanwhile, the transferred excitons contribute to the population redistribution of acceptor states, especially the 2S exciton state. Therefore, the competition between FRET-mediated exciton transfer and Auger recombination influences on determining the exciton population dynamics and the establishment of favorable gain conditions for 2S-state lasing.

Reference

[1] Basu P K, Mukhopadhyay B and Basu R 2022 *Semiconductor Nanophotonics* (Oxford: Oxford University Press) pp.292–327.
[2] Chou K and Dennis A 2015 *Sensors* **15** 13288.
[3] Montanarella F, Biondi M, Hinterding S, Vanmaekelbergh D and Rabouw F 2018 *Nano Lett.* **18** 5867.
[4] Ahn N, Livache C, Pinchetti V and Klimov V 2023 *Chem. Rev.* **123** 8251.
[5] Cragg G E and Efros A L 2010 *Nano Lett.* **10** 313.